Composites Science and Technology 166 (2018) 115–124

Contents lists available at ScienceDirect

Composites Science and Technology

journal homepage: http://www.elsevier.com/locate/compscitech

# Strong process-structure interaction in stoveable poly(urethane-urea) aligned carbon nanotube nanocomposites

Jeffrey L. Gair Jr. [a, b, c], Robert H. Lambeth [a], Daniel P. Cole [a], Dale L. Lidston [c], Itai Y. Stein [c], Estelle Kalfon-Cohen [c], Alex J. Hsieh [a], Hugh A. Bruck [b], Mark L. Bundy [a], Brian L. Wardle [c, *]

[a] U.S. Army Research Laboratory, Aberdeen Proving Ground, MD, 21005-5069, USA
[b] Department of Mechanical Engineering, University of Maryland, College Park, MD, 20742, USA
[c] Department of Aeronautics and Astronautics, Massachusetts Institute of Technology, Cambridge, MA, 02139, USA

ARTICLE INFO

*Article history:*
Received 2 September 2017
Received in revised form
30 January 2018
Accepted 9 February 2018
Available online 3 March 2018

ABSTRACT

The exceptional static and dynamic physical properties of poly(urethane-urea) (PUU) elastomers make them prime candidates for impulsive loading structural applications, such as blast protection coatings. Since the theoretical physical properties of carbon nanotubes (CNTs) are among the best for any currently known material, a number of previous studies explored the use of CNTs as nanoscale fillers to enhance the properties of PUU nanocomposites. However, due to the challenges inherent in dispersing CNTs in a PUU matrix and the resulting random orientation of the CNTs, these previous works observed marginal improvements in physical properties, and were unable to establish clear structure-property relations. Here, we report the synthesis of aligned-CNT (A-CNT) reinforced PUU polymer nanocomposites (A-PNCs) by infusing A-CNT forests with a stoveable PUU, and establish process-structure-property relations that quantify the contribution of CNT confinement on the PUU mechanical response. This stoveable process was achieved using blocked isocyanate which prevented polymerization until the blocks were removed with heat. PUUs of two distinct compositions were explored: one with 40 wt% hard-segment content (PUU211) and the other with 66 wt% hard-segment content (PUU541). Thermogravimetric analysis indicates that A-CNTs enhance the thermal stability of the hard-segment phase in PUU A-PNCs at 340 °C by up to 45% over the baseline PUUs. Atomic force microscopy reveals that the elongated nanophase hard-segment formations along the CNT axis observed only in the nanocomposites were of similar characteristic size to the average inter-A-CNT spacing (~70 nm), indicating a strong influence of A-CNTs on the size and orientation of hard-segment nanophases, as corroborated via small angle X-ray scattering. Nanoindentation testing reveals that PUU A-PNCs possess significant elastic anisotropy, and exhibit enhanced longitudinal effective indentation moduli of ~460 MPa (>3 × that of the PUU211 baseline) and ~1350 MPa (~1.5 × that of the PUU541 baseline) for PUU211 and PUU541 nanocomposites, respectively. This difference in magnitude of CNT reinforcement efficacy indicates that CNT confinement leads to significant hard-segment re-organization in the PUU211 A-PNCs, whereas the interconnected network of hard-segments in the PUU541 is affected by CNT templating to a lesser extent. Dynamic nanoindentation testing results are consistent with these interpretations, where longitudinally-loaded PUU211 A-PNCs are found to exhibit a >3 × enhancement in storage modulus at 1 Hz of ~730 MPa, whereas the longitudinally-loaded PUU541 A-PNCs exhibit a slightly enhanced storage modulus enhancement at 1 Hz of 2190 MPa (~1.5 × that of the PUU541 baseline). Reinforcement of PUUs with A-CNTs is a promising way to tune the physical properties of the PNCs; higher A-CNT packing densities, where the inter-CNT spacing could approach the nanophase characteristic diameter, could further enhance the PUU performance in ballistic protection applications.

© 2018 Elsevier Ltd. All rights reserved.

* Corresponding author. Tel.: +1 617 252 1539.
*E-mail addresses:* jeffrey.l.gair.ctr@mail.mil (J.L. Gair), wardle@mit.edu (B.L. Wardle).

https://doi.org/10.1016/j.compscitech.2018.02.011
0266-3538/© 2018 Elsevier Ltd. All rights reserved.

## 1. Introduction

The high hardness, flexibility, tear and tensile strength, and chemical and water resistance of poly(urethane-urea) (PUU) elastomers makes them desirable for use in material architectures for high-value applications such as ballistic protection [1–6], medical implants [7–9], and structural and composite reinforcement [6,9,10]. To further enhance the properties of PUUs, many previous studies have explored the incorporation of nano-scale fillers, especially carbon nanotubes (CNTs), into PUUs, which form polymer nanocomposites (PNCs) [11–13]. Such randomly-oriented PNCs were investigated for a variety of physical property enhancements, including mechanical [14,15], thermal [16,17], and electrical [18] properties. However, PUU-based PNCs typically exhibit significant amounts of phase separation due to aggregation of the nano-fillers, which culminates in marginal improvements in physical properties, and unclear structure-property relations [15,19,20]. Common approaches for producing well dispersed PNCs, such as high-speed mixing, surface functionalization, and sonication [12,21], can be extremely harsh and are known to induce defects in the nano-fillers, such as sonication-induced scission [22–24], which could diminish the intrinsic properties of the nano-fillers and limit PNC properties [25]. These PNC manufacturing challenges can be mitigated by infusing the polymer matrix directly into a free-standing architecture, such as vertically aligned CNTs (A-CNTs). This was previously shown not to damage the underlying CNTs, to maintain their original alignment (*i.e.*, no aggregation), and allow high CNT volume fraction ($V_f$) in the PNCs [25]. Here, we synthesize A-CNT/PUU PNCs by infusing A-CNTs (sometimes referred to as CNT forests, CNT arrays, vertically-aligned CNTs, etc.) with two types of stoveable PUUs, and develop process-structure-mechanical property relations which quantify how CNT confinement alters the two PUU matrices.

Since PUU is a biphasic polymer comprising both urethane and urea linkages, a broad range of properties similar to both polyurethane and polyurea can be realized [2]. The monodentate hydrogen bonds formed by urethane groups are relatively weak, giving rise to softer linkages, while the bidentate bonds from ureas provide more rigid linkages [26]. By incorporating these two types of bonds in various proportions, a wide range of mechanical properties are achievable. PUU is attractive because it offers relative ease of manufacturing [26], advantageous mechanical properties [27], and excellent tunability [28]. Extensive work has been done to study the effects of phase-mixing, in terms of quasi-static [27], dynamic [29], and microstructural [9,26,30,31], properties. It was demonstrated that varying stoichiometric ratios of isocyanate, chain extender, and polyol, as well as adjusting the polyol molecular weight, leads to a wide range of tunable mechanical properties [28,29], making them very attractive for the present work. Additionally, achieving thermoplastic or thermoset behavior is also feasible via such stoichiometric variation, offering an additional range of tunability.

PUU offers tunability and durability as a matrix material for composite structural applications, however polymer synthesis has presented a challenge for infusion into CNT forests to form PUU aligned polymer nanocomposites (A-PNCs). In practice, the rapid rate of polymerization in PUU prohibited fabrication of A-PNCs. Not only does the reaction occur too rapidly to adequately wet the CNT forests, but the diisocyanate reacts with water adsorbed onto the surfaces of the CNTs [32], resulting in off-gassing. This combined with rapid set time results in voids, and thus, unsuitable A-PNCs. To overcome this, a PUU synthesis method involving blocked diisocyanate was employed, permitting complete wetting and saturation of the CNT forests prior to completion of polymerization. A schematic of the PUU synthesis process can be found in Fig. 1(a). By capping the isocyanate groups with nonreactive blocks,

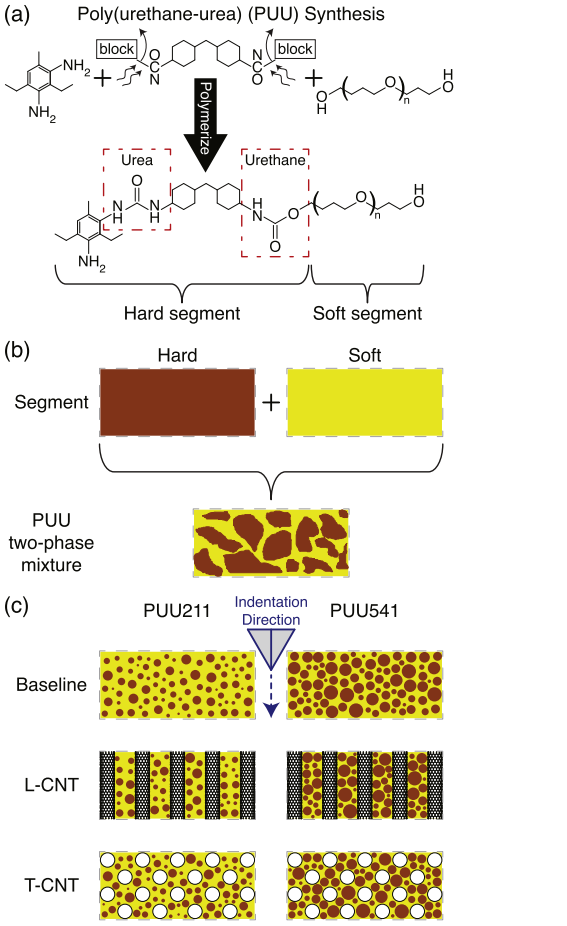


**Fig. 1.** Overview of poly(urethane-urea) (PUU) synthesis and reinforcement with aligned carbon nanotubes (A-CNTs) to form aligned-CNT polymer nanocomposites (A-PNCs). (a) Schematic of stoveable synthesis of PUU. (b) Biphasic nature of hard and soft segments in PUU. (c) Diagram of PUU211 and PUU541 in baseline, and A-PNCs with longitudinally-oriented CNTs (L-CNTs) and transversely-oriented CNTs (T-CNTs). Orientation corresponds to the typical composite principal material directions and aligns with the axis of nanoindentation as shown.

polymerization is prevented. These blocks can then be removed with heat, allowing the PUU to be stoveable. These blocking groups are then released from the material, followed by rapid polymerization, resulting in a typical PUU polymer. Polymerization results in the formation of hard and soft phases as seen in Fig.1(b).

This work explores the degree of morphological and mechanical tunability of PUU A-PNCs with a view to transition to structural composite applications, particularly microfiber-based advanced composites such as carbon fiber reinforced plastics. Here the relationship between the structure and morphology of A-CNTs and the molecular arrangement of *in situ* polymerized PUU is quantified. To understand the effects of hard and soft segment composition, two stoichiometric species of PUU are investigated as shown in Fig. 1(c), which reveals not only any predilection for CNT interaction with one of the PUU segments, but also the tunability of the mechanical properties. By elucidating the mechanisms controlling mechanical properties for these PUU composites, this work paves the way for the design and fabrication of PUU-based composite structures with tuned mechanical behavior for a wide range of applications.

## 2. Methods

PUU synthesis and A-PNC fabrication are described, followed by

characterization and mechanical testing procedures.

### 2.1. Poly(Urethane-urea) synthesis

Poly(urethane-urea) (PUU) was synthesized using a blocked-HMDI (Desmodur BL5375, Covestro) as the diisocyanate, DETA (Ethacure 100-LC, Albemarle) as the diamine, PTMO (PolyTHF 650, BASF) as the polyol, and a tin catalyst (DBTL). The use of 0.3 wt% DBTL was per the blocked-HMDI manufacturer recommendations for reducing unblocking temperature. The materials were weighed and mixed via an overhead stirrer, then degassed at 2 kPa for 30 min. This PUU prepolymer was then poured into molds and cured for 24 h at 130 °C. Two stoichiometric variations of PUU were used in this work: a 2:1:1 ratio of HMDI:DETA:PTMO and a 5:4:1 ratio species. These were named PUU211 and PUU541 respectively. The naming scheme for baseline and A-PNCs with both transversely-oriented CNTs (T-CNTs) and longitudinally-oriented CNTs (L-CNTs), molar ratios, and resultant compositions of hard and soft segments are provided in Table 1. The T-CNT PNCs and L-CNT PNCs are fabricated identically; this designation refers only to principal material directions (and thus the orientation of sectioning for nanoindentation).

The 130 °C cure temperature was determined based on the unblocking temperature of the HMDI from the manufacturer and the known degradation temperatures of the constituents. The 24 h cure time could not be determined implicitly due to the complexity of the reaction kinetics; and so it was determined based on a cure study involving thermogravimetric analysis (TGA), differential scanning calorimetry (DSC), and attenuated total reflection (ATR) analysis of PUU211 and PUU541, both neat and A-PNCs. Specimens were cured for 12, 18, 24, or 28 h at 130 °C, and post-cured for 0, 15, 30, 45, and 60 min at 210 °C. 24 h at 130 °C with no post-cure was found to push the cure of all materials to ~100% without introducing confounding variables or exposure to potentially damaging heat [33].

### 2.2. A-PNC fabrication

A thermal catalytic chemical vapor deposition process at atmospheric pressure was used to synthesize, or “grow”, aligned CNTs (A-CNTs) in a quartz tube with inner diameter of 22 mm, as described previously [17,34,35]. These multiwalled (3–7 walls) A-CNTs were grown on a 1 cm × 1 cm Si substrate using Fe catalyst on alumina support. They had an outer diameter of ~8 nm, an inner diameter of ~5 nm [35,36], and were spaced, on average, at ~ 70–80 nm apart [37–40]. The A-CNTs had a height of ~5 mm, and a volume fraction ($V_f$) of ~1% [35].

PUU A-PNCs were fabricated by impregnating the A-CNT forests with the mixed and degassed PUU prepolymer, and then curing the PUU using the cure conditions described in Section 2.1. Once the PUU was mixed, it was degassed at ~2 kPa until foaming subsided. After this, the A-CNT forests were fully submerged in the PUU and degassed at ~2 kPa for an additional 60 min. The uncured A-PNCs were placed on an aluminum plate carrier substrate for curing in a nitrogen-filled oven.

To achieve smooth and flat specimen surfaces for AFM imaging and nanoindentation tests, samples were ultra-cryotomed at −70 °C using a Leica Ultracut UCT with a cryo-chamber. Neat PUU resin specimens, as well as T-CNT and L-CNT samples, were prepared in order to gain insight into the potential CNT-induced phase orientation and inherent anisotropy of the A-PNCs. A-PNC samples were cut and placed into AFM holders, which maintained CNT orientation and provided a suitable platform for holding and positioning specimens during cryotome, and subsequently, AFM and nanoindentation. Care was taken to characterize the center of the CNTs along their length, as morphology of the CNTs may vary towards the top and bottom of the forests. To this end, T-CNT samples were sectioned longitudinally at the center of the 1 cm × 1 cm forest and L-CNT samples were sectioned transversely at a height of ~2.5 mm.

### 2.3. Microstructural characterization

TGA was performed using a TA Instruments Discovery TGA. Temperatures were ramped from 23 °C to 500 °C at 10 °C/min. in air. Scanning probe microscopy measurements were conducted using an Asylum Research Cypher AFM. A silicon tip with a natural frequency of 70 kHz and stiffness of 2 Nm was used to perform alternating contact mode scans at a scan rate of 0.6 Hz. Small angle X-ray scattering (SAXS) experiments were performed with a Rigaku MicroMax-007HF. A Cu K-alpha source (wavelength $\lambda = 0.154$ nm) at 40 kV and 30 mA was used. The distance between the sample and the detector was 1525 mm. Baseline specimen orientation was inconsequential, however A-PNC specimens were positioned such that the beam would pass parallel with the axes of the A-CNTs. This would maximize the ability to observe the signal passing between the CNTs, which have an average inter-CNT spacing ~60–80 nm [35,37,39], and would prevent scatter from CNT directionality.

### 2.4. Nanoindentation

Quasi-static and dynamic nanoindentation experiments were performed on a Hysitron TI950 Triboindenter with a diamond Berkovich tip having a radius of curvature ~150 nm. Specimens were kept in the AFM holders in which they were cryotomed in order to provide an indentation surface normal to the indentation direction.

Quasi-static load functions were tuned for PUU211 materials and for PUU541 materials separately as the stiffnesses of each polymer dictated different loading conditions in order to engage similar contact area. Both quasi-static load functions had a 5 s ramp up, 5 s hold, and 5 s ramp down. The hold is necessary to account for anelastic behavior in determining elastic indentation modulus. The max force for each was determined based on the force required to achieve a ~1 μm indentation depth, as this would reduce noise and effects of surface variation. Nanoindentation tests were performed in load-controlled mode with a loading rate of 40 μN/s for PUU211 and 60 μN/s for PUU541. For all quasi-static tests, an array

**Table 1**
PUU and A-PNC naming scheme, molar ratios, and compositions of hard and soft segments (Hs and Ss respectively).

| Nomenclature | CNT Orientation | Ss wt.% | Hs wt.% | Molar Ratios (HMDI:DETA:PTMO) |
|---|---|---|---|---|
| PUU211 | - | 60% | 40% | 2:1:1 |
| T-CNT/PUU211 | Transverse | 60% | 40% | 2:1:1 |
| L-CNT/PUU211 | Longitudinal | 60% | 40% | 2:1:1 |
| PUU541 | - | 34% | 66% | 5:4:1 |
| T-CNT/PUU541 | Transverse | 34% | 66% | 5:4:1 |
| L-CNT/PUU541 | Longitudinal | 34% | 66% | 5:4:1 |

of 16 points spaced 5 μm apart were tested at each of 3 positions on the specimen surface, resulting in 48 quasi-static indentation tests per specimen. Two separate specimens were tested for each sample type to confirm repeatability of sample fabrication and preparation, yielding a total of 96 indents for a given sample type.

Dynamic load functions were also tuned for PUU211 vs. PUU541 materials. The load functions were similar to quasi-static load functions with the substitution of a dynamic loading sequence *in lieu* of the hold segment. During this dynamic sequence, the specimen surface was indented at 1–200 Hz in increments of 10 Hz for 200 cycles at each frequency. The order of frequency was randomized to reduce artifacts. The desired dynamic amplitude required to overcome noise and surface variability is ~5 nm; and so dynamic loads for PUU211 and PUU541 materials were set to 3 μN and 50 μN, respectively. Tests were run at 3 positions on the surface of each specimen, each of which comprising 9 test points spaced 5 μm apart for a total of 27 dynamic indentation tests per specimen. Two separate specimens were tested for each sample type to confirm repeatability of sample fabrication and preparation, yielding a total of 54 indentation positions for a given sample type.

## 3. Results & discussion

The techniques for structural quantification described in the previous section are utilized along with mechanical characterizations to establish process-structure-property relations for the A-PNCs.

### 3.1. Microstructural characterization

Characteristic TGA results are displayed in Fig. 2(a). Notice that all curves agree very well with one another until ~340 °C, indicating identical thermal degradation behavior prior to this point. Notice also that the plateau values above 475 °C also agree, though the PUU211 A-PNC and PUU541 A-PNC curves finally settle at ~15% and ~13% respectively, approximately 5% and 3% above their neat counterparts. This elevation cannot be ascribed solely to the CNT weight fraction, as this accounts for only ~1 to 2 wt% (these A-CNTs were found to have an intrinsic density of ~1.6 g/cm$^3$) [35], indicating that the A-CNTs have slightly improved the thermal stability of the PUU at this high-temperature range, likely due to an alteration in the polymer local to the CNTs. From 325 °C to 475 °C the four materials each exhibit similarly shaped curves with definitive features. From the upward shift of PUU211 and PUU541 in A-PNCs over their neat counterparts, it is evident that the A-CNTs stabilize the thermal degradation in this temperature range.

There are two distinct regions of rapid drop in residual mass: the first located at 335 °C ($T_I$) and the second at 440 °C ($T_{II}$). The PUU211 loses ~40% of its weight after $T_I$, while the PUU541 loses ~60%, corresponding to the weight percent of hard segments for each (see Table 1). After $T_{II}$ however, both PUU211 and PUU541 have lost 90% of their weight, with PUU211 losing ~50% of its weight and PUU541 losing 30% after $T_{II}$. These values match closely to the relative composition of soft segments for each neat PUU. The proportions suggest that pyrolyzation of hard segments is responsible for the degradation up to 350 °C, after which soft segments begin to degrade. Similar data supporting the pyrolyzation of hard segments at lower temperatures and soft segments at higher temperatures have been seen elsewhere [16,41]. To further investigate the nature of thermal degradation between $T_I$ and $T_{II}$, the derivative of wt.% has been plotted in Fig. 2(b). Because the rate of degradation is directly proportional to the mass lost over a temperature range during a constant temperature ramp, the relative sizes of peaks seen in Fig. 2(b) reveal compositional degradation ratios. The conclusion that $T_I$ is associated with hard segment pyrolysis and $T_{II}$ with soft segment pyrolysis is supported in the derivative plot. More interesting is the apparent thermal stabilization of PUU by the A-CNTs. In both PUU211 and PUU541, A-PNC residual mass is greater than its baseline counterpart between $T_I$ and $T_{II}$, as seen in Fig. 2(a). Furthermore, Fig. 2(b) reveals a substantial reduction in rate of degradation in the presence of A-CNTs during hard-segment pyrolyzation, but acceleration of soft-segment degradation. A similar CNT affinity for hard-segment interaction was found elsewhere [42], and has been found to occur to a greater degree in *in situ* polymerized polyurethanes [43]. It is possible that this stabilization arises from the formation of an interphase region at the surface of A-CNTs. This is supported by AFM images where a clear effect may be found between the presence of the A-CNTs and the ordering of the PUU matrix (Fig. 3).

Fig. 3(a), 3(c), and 3(e) provide AFM height images for neat PUU211, transversely-oriented PUU211 A-PNC (T-CNT/PUU211), and longitudinally-oriented PUU211 A-PNC (L-CNT/PUU211). Fig. 3(b), 3(d), and 3(f) contain the corresponding phase images. When comparing the amorphous nature of the PUU211 (Fig. 3(a) and 3(b)) with the highly-ordered, anisotropic nature of the T-CNT/PUU211 (Fig. 3(c) and 3(d)), it is clear that the CNTs have not only induced nanophase ordering, but also orientation of these phases along the direction of the CNTs. These nanophases are found to be ordered hard-segments; the brighter representation in AFM phase images indicates stiffer phases [44,45]. The large (60% by weight) soft-segment content of PUU211 allows enough freedom of hard-segment movement to permit the formation of these domains during the cure cycle. AFM images of longitudinally-oriented PUU211 A-PNCs (L-CNT/PUU211) can be found in Fig. 3(e) and 3(f), and revealed small circular phases rather than the elongated structures present in T-CNT/PUU211. This indicates that these hard-segment domains are shaped by the surrounding CNTs. Highly-ordered nanophases were less visible in PUU541 A-PNCs (see Supplementary Materials Fig. S1). This is likely because the relatively low (34% by weight) soft-segment content of PUU541 is insufficient to permit free movement of hard-segments during the curing process, decreasing aggregation in the cured A-PNC. A similar reduction in aggregation due to restricted movement was observed by Fernandez-d'Arlas, who studied the interactions between multi-walled CNTs and polyurethanes [42]. However, phases observed in the PUU541 A-PNC were ~10 × smaller than those in the neat PUU541. This is likely due to reduced phase aggregation arising from low chain mobility due to the presence of the A-CNTs.

SAXS complements and corroborates the observations of hard and soft phase morphology from AFM by giving information on feature sizes and their relative proportion. Characteristic SAXS results can be seen in Fig. 4(a) and Fig. 4(b) for PUU211 and PUU541 materials respectively. In Fig. 4(a), the PUU211 sample has a very gradual slope which indicates high levels of phase-mixing, while the sharper peak found in the PUU211 A-PNC is indicative of greater phase-separation [28,31,46]. This CNT-induced phase-separation observed from SAXS supports findings from TGA and AFM. A similar trend can be seen in Fig. 4(b) for the PUU541 materials. Note that the transition from large to small feature size (low to high values of scattering vector, $q$) is more linear for PUU541 materials than the PUU211 materials, indicating a greater variety of phase sizes in the PUU541. This difference between the PUU211 and PUU541 is consistent with the restricted mobility which arises from greater hard segment content in the PUU541 [42]. Note that greater phase-separation has not led to larger phase sizes, but in fact shifted the peaks of the A-PNC curves towards smaller feature sizes. This indicates that A-CNTs induce phase-separation but restrict aggregation of large phases, supporting observations from AFM.

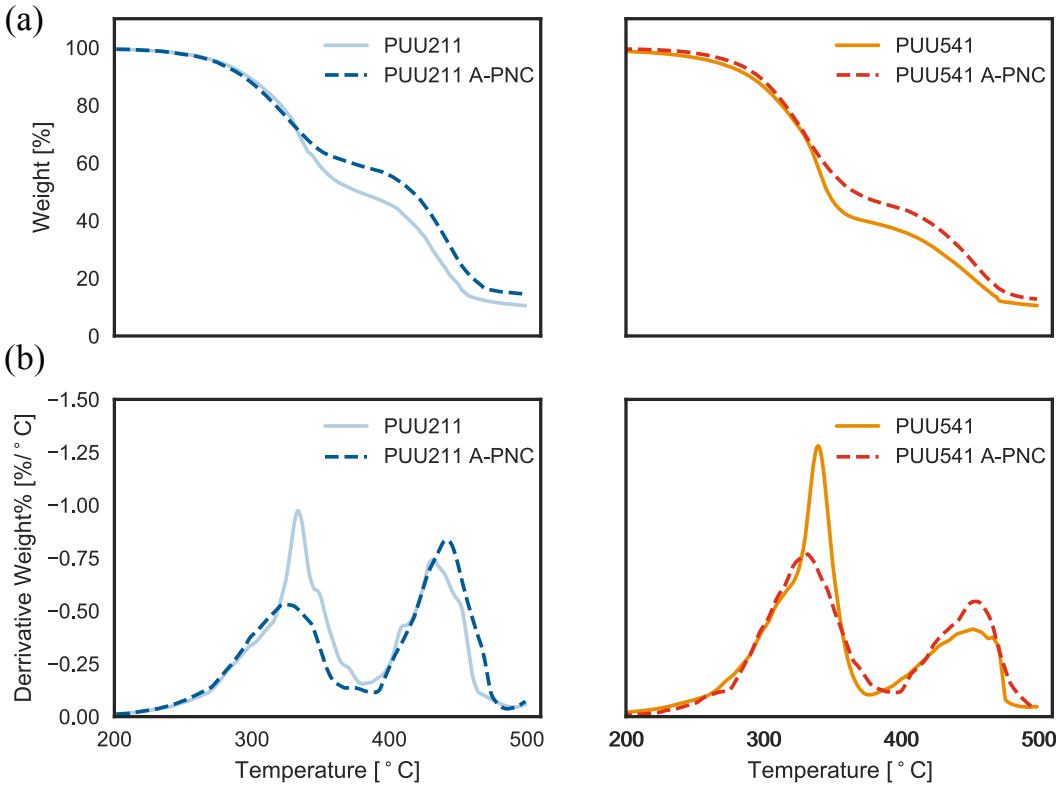


**Fig. 2.** Thermogravimetric analysis (TGA) of neat PUU and A-PNC materials: (a) Residual mass vs. temperature plot showing that large mass losses occur at ~335 °C and ~440 °C, and that A-PNCs exhibit greater thermal stability. (b) Derivative of residual mass with respect to temperature corroborating that A-PNCs exhibit more thermal stability compared to the baseline PUUs.

### 3.2. Microscale mechanical characterization

Measurement of the indentation modulus is taken from the slope of the unloading curve according to previous work [47], which was then corrected for anelastic effects following prior work [48,49]. The term indentation modulus is used here *in lieu* of reduced elastic modulus due to the anisotropy of the materials [50]. Average quasi-static data for PUU211 and PUU541 materials can be found in Fig. 5 and in tabulated form in the Supplementary Materials (Table S1); standard error has been calculated based on 96 test positions. The PUU211 has the lowest indentation modulus of 152 ± 3.7 MPa, followed by the T-CNT/PUU211 with 211 ± 7.4 MPa, and then the L-CNT/PUU211 with 461 ± 9.2 MPa. CNT-reinforced PUU211 A-PNCs exhibit a higher modulus, which is expected due to the reinforcing nature of the stiffer (relative to the PUU) CNTs. The observation that T-CNT/PUU211 has a lower indentation modulus than the L-CNT/PUU211 likely arises from the combination of two effects: the orientation of A-CNTs and the orientation of nanophases. Compression of the A-CNTs perpendicular to their alignment direction is governed by a much smaller intrinsic CNT modulus (~1 GPa in the transverse direction vs. ~ 1 TPa for the longitudinal direction) [38,51], and the orientation of the CNT-induced nanophases observed *via* AFM have been shown to offer additional reinforcement. This shared enhancement was modeled and will be discussed below. A similar trend was found in PUU541 materials. The PUU541 has the lowest indentation modulus of 920 ± 5.1 MPa, followed by the T-CNT/PUU541 with 1040 ± 7.1 MPa, and then the L-CNT/PUU541 with 1350 ± 11 MPa. These moduli are significantly higher than those recorded for the PUU211 materials, which is to be expected since the PUU541 has a 66% hard phase composition while the PUU211 only has a 40% hard phase composition. This may indicate that the hard-segment content of the PUU541 is high enough to form interconnected networks of hard domains. Furthermore, the indentation moduli increases are smaller but statistically significant when comparing baseline and A-PNCs with T-CNTs, confirming that similar mechanisms are a play. This is a reasonable conclusion since the matrix material should dominate transverse loading. Similar anisotropic properties were observed and characterized elsewhere [51]. The enhancement to indentation modulus by the CNTs is profound, particularly in the case of the PUU211. The A-CNTs offered a 49% improvement to PUU211 indentation modulus in the transverse direction and a 225% improvement in the longitudinal direction, resulting in an anisotropy ratio of 2.2. By comparison, the A-CNTs offered only a 13% enhancement to indentation modulus for PUU541 in the transverse direction and 47% in the longitudinal direction, with an anisotropy ratio of only 1.3. The observed indentation modulus enhancement is greater than that which the rule of mixtures predicts, as described by the model below. It is reasonable that the improvement is greater in the softer PUU211 than the PUU541 since there is a greater disparity between the stiffnesses of the CNTs and the matrix. The load is transferred from the softer matrix to the stiffer CNTs to a greater degree because of this mismatch, giving rise to a larger reinforcement of the PUU211. This type of load transfer from lower-modulus materials to higher-modulus fillers is seen in many composites, including nanocomposites [52]. Furthermore, the presence of hard-segment nanophases aligned and oriented parallel to the axes of the A-CNTs in the PUU211 and not in the PUU541 could be a major contributor to the greater improvement seen in the PUU211 materials. Nonetheless, in each case, the A-CNTs oriented longitudinally offered ~4 × more enhancement to indentation modulus than in the transverse direction.

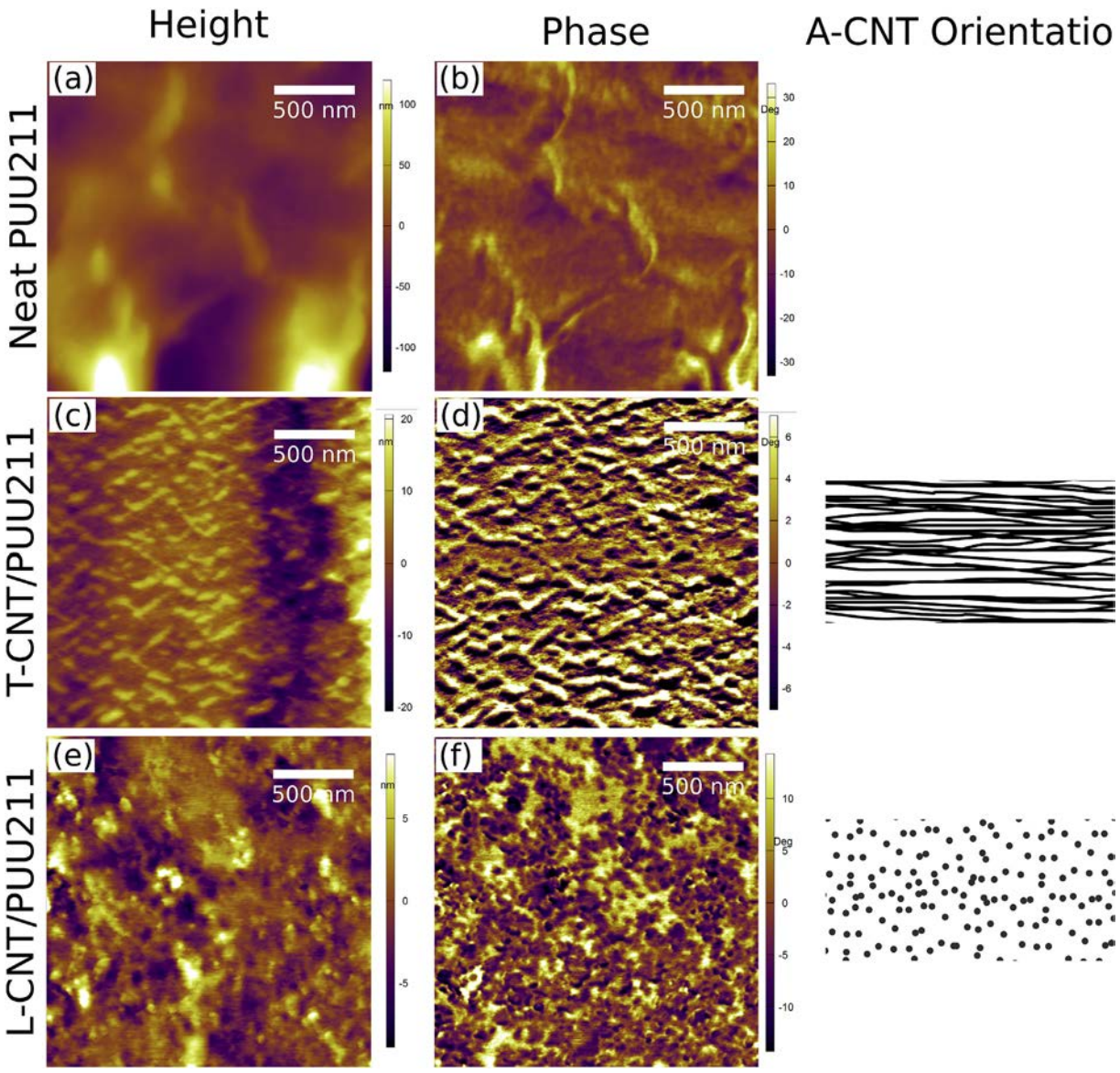


**Fig. 3.** Representative AFM height (in nm) and phase (in degrees) images: PUU211 (a) height, (b) phase; T-CNT/PUU211 (c) height, (d) phase; L-CNT/PUU211 (e) height, (f) phase.

Recent work on A-CNT arrays, similar to the ones used here, with $V_f$ ranging from ~1 to 20 vol % found that the indentation derived effective modulus ($E_{eff}$) of the A-CNT array ranged from ~1 MPa to ~ 1 GPa [50], which is consistent with other previous works on indentation of A-CNT arrays [53–56]. Such an enhancement in $E_{eff}$ in CNT arrays of higher $V_f$ is likely a combination of CNT collective reinforcement in CNT-CNT junctions [57–59], and a reduction in CNT waviness that results from densification [38,39,60]. Stein et al. [38] modeled how waviness scales the $E_{eff}$ of the stochastic CNTs that comprise the CNT arrays, and found that a waviness ratio of ~$0.2 \pm 0.1$ for CNTs at $V_f$ ~ 1%, similar to the ones studied herein, reduced the $E_{eff}$ of the CNTs by between $10^3 \times$ to $10^5 \times$ when compared to the intrinsic longitudinal modulus of ideal and perfectly straight CNTs (~1 TPa). The intrinsic transverse modulus of perfectly straight CNTs is much smaller, and was found to have a value of ~1 GPa for these CNTs in previous work [38]. This large reduction in $E_{eff}$ originates from the >90% compliance contribution of the torsion and shear deformation mechanisms in A-CNT arrays [38]. Two ways to significantly enhance $E_{eff}$ of CNT arrays include reducing the CNT waviness and restricting CNTs from translating and rotating with respect to one another (which was previously assumed to effectively eliminate the torsion deformation mode [51]), both of which occur during infusion and subsequent curing of the polymer matrix [51,60,61]. Based on the effective modulus contribution of 1 vol % CNTs (as-grown A-CNT forests), a modulus of ~3 GPa can be used to compute the PNC $E_{eff}$ using rule of mixture. The following rule of mixture computations are based on measured $E_I$ (indentation modulus) for the neat PUU211 and PUU541 polymers respectively. Considering 1 vol % CNTs ($E_{eff}$ ~ 3 GPa) [40], and PUU211 as the matrix ($E_{eff}$ 152 MPa), rule of mixtures predicts $E_{eff}$ ~ 180 MPa for L-CNT/PUU211 which is less than half that of the 461 MPa obtained experimentally. Since $E_{eff}$ supposes no confinement effects, and perfect binding between the CNT and the polymeric chain, we can conclude that the ~60% under-prediction noted here arises from the morphology of the matrix and its interaction with the CNTs. For PUU541 with $E_{eff}$ of 920 MPa, rule of mixture predicts $E_{eff}$ ~940 MPa for L-CNT/PUU541, which is only a ~30% under-prediction of the ~1350 MPa obtained

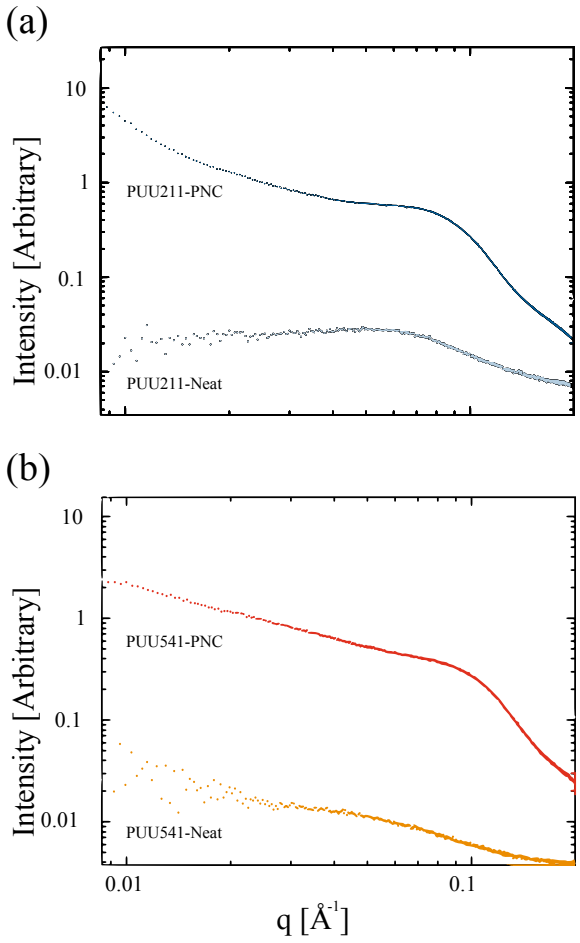


**Fig. 4.** Small-angle X-ray scattering (SAXS) intensities as a function of scattering vector (q) for baseline PUUs, and PUU polymer nanocomposites (A-PNCs). (a) PUU211, (b) PUU541.

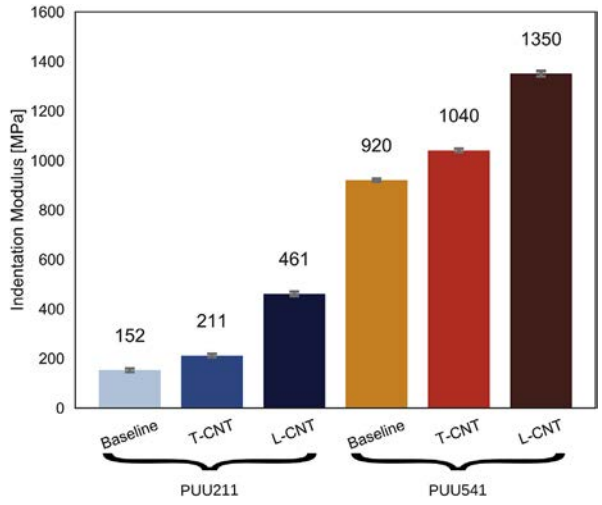


**Fig. 5.** Summary of quasi-static nanoindentation data comparing average indentation moduli for all materials tested.

experimentally. This is likely due to a greater concentration of hard-segments in the PUU541, potentially aiding in the formation of interconnected hard-segment networks, reducing dependency on A-CNTs to form these networks. These significant enhancements found in the A-PNCs may also originate from the polymer having properties different than the neat matrix in the presence of the A-CNTs, i.e. process-structure changes due to the A-CNTs. This leads to polymer ordering and/or orientation local to the CNT surface, possibly changes in the crystallinity of the nanophase regions, and additional crystallite templating and other meso-scale effects [4]. These results show that CNT reinforcement purely accounts for <10% of the observed enhancement in PUU211 and PUU541 reinforced with L-CNTs, which indicates that phase evolution and formation of preferential texture within these PUU matrix materials is a likely explanation that requires further quantification and modeling in future work.

The dynamic nanoindentation data for PUU211 and PUU541 materials is presented in Fig. 6, where standard error has been calculated based on 54 test positions. The trend from quasi-static data of PUU211 and PUU541 A-PNCs being stiffer continues in the dynamic tests: storage and loss moduli in the longitudinal direction are higher for these materials. Further, the improvement to storage moduli offered by A-CNTs is more pronounced in the softer PUU211 than the PUU541, similar to the quasi-static nanoindentation tests. The PUU541 has a storage modulus which is nearly 8 × greater than that of PUU211, so the contribution offered by the CNT reinforcement is only ~ +50% in L-CNT/PUU541 compared to the ~ +300% in the case of the L-CNT/PUU211. Note also that the CNTs' improvement to storage modulus is slightly less at 200 Hz than at 1 Hz. This is presumably due to the rate-sensitivity of the soft segments in the matrix, leading to greater dynamic stiffening at higher frequencies. The PUU211 sees a ~120% increase in storage modulus from 1 to 200 Hz, while the PUU541 only exhibits a 26% increase in storage modulus from 1 to 200 Hz. This is consistent with the soft segments of the matrix contributing to rate-sensitivity and exhibiting rate-induced stiffening. Because the matrices stiffen at higher rates, they offer a greater contribution in the A-PNCs, lessening the degree of enhancement from the CNT $E_{eff}$ stiffness. Notice that the storage modulus enhancement from low to high rates is most pronounced in the neat PUUs, followed by the A-PNCs with transverse CNTs, and then lastly the A-PNCs with longitudinal CNTs; precisely the opposite progression as is seen in indentation and storage moduli. This is to be expected, as the matrix is more rate-sensitive than the CNTs, and the matrix dominance decreases respectively in those materials. CNTs are also found to increase the loss moduli. These observations continue the trend that CNT improvements are greater in the softer PUU211 and in the longitudinal orientation.

Tanδ (loss/storage) plots can be found in Fig. 6(b). All the materials exhibit rate-insensitive tanδ, a property indicative of the extent of phase-separation in these PUU materials [9]. The highest tanδ can be found in PUU211, followed by both PUU211 A-PNCs which have similar tanδ behaviors. The PUU211 has a much greater tanδ than traditionally synthesized PUU211 [9]. This could be due to greater phase-separation, leading to improved loss modulus, and thus tanδ. The fact that the T-CNT/PUU211 and L-CNT/PUU211 have similar tanδ values despite different storage moduli indicates proportional improvements to both storage and loss moduli for each. It can be concluded that A-CNTs work to increase both storage and loss moduli, where greater enhancement is noted in the storage modulus. This is a reasonable conclusion, as the A-CNTs act to restrict mobility of soft-segment domains, improving stiffness and preventing the chain slippage and detanglement associated with loss. Note that tanδ curves for all PUU541 materials are clustered together (within standard error) despite having significantly different storage and loss moduli. From this it is clear that A-CNTs improve storage and loss approximately equally in PUU541.

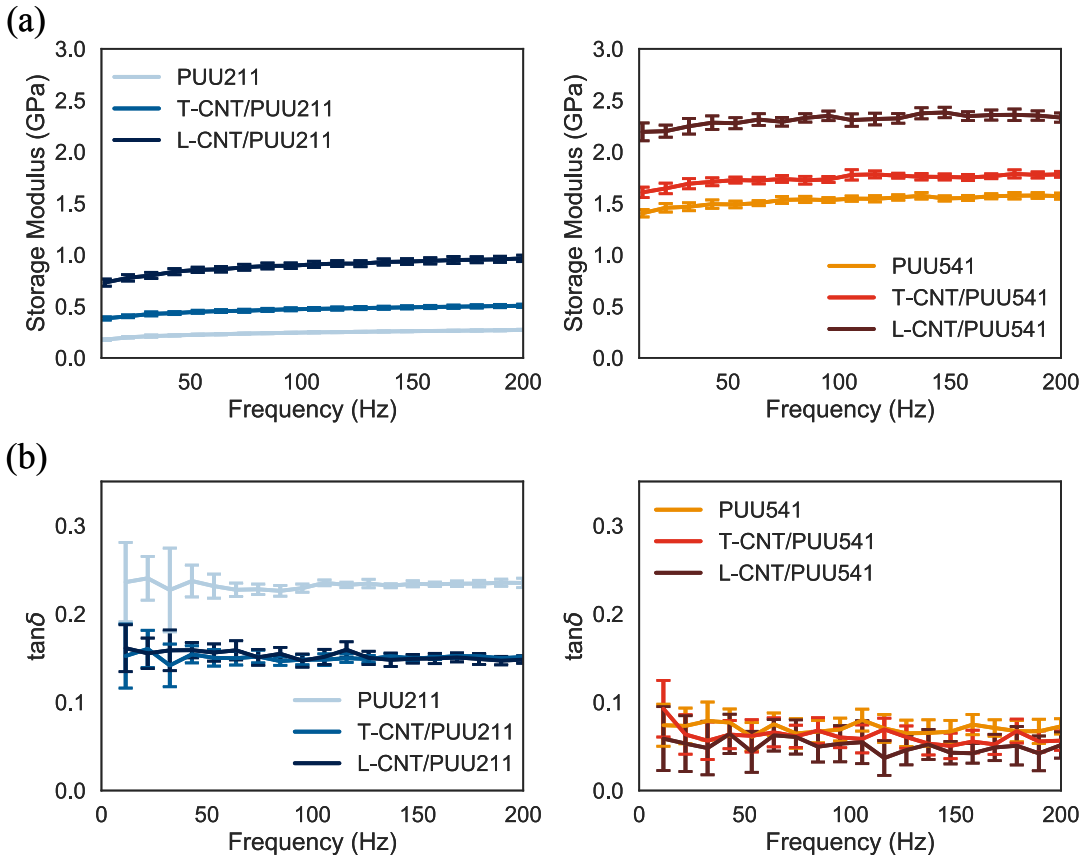


**Fig. 6.** Summary of dynamic nanoindentation data with standard error for PUU211 and PUU541 baseline and PNC materials. (a) Storage moduli comparison. (b) tanδ comparison.

## 4. Conclusions

In summary, process-structure-mechanical property relations for poly(urethane-urea) (PUU) elastomers reinforced with aligned carbon nanotubes (A-CNTs) were established for two distinct PUU matrix materials: one with 40 wt% hard-segment content (PUU211) and the other composed of 66 wt% hard-segment (PUU541). Thermogravimetric analysis revealed identical thermal degradation up to 340 °C for both PUU211 and PUU541 polymer nanocomposites (A-PNCs), and that there are two major spikes in thermal degradation: one at 340 °C and one at 440 °C, which are attributed to hard-segment and soft-segment degradation respectively. These results suggest that A-CNTs stabilize the thermal degradation of PUU hard-segments, and since CNTs account for ~1–2% of the weight of the A-PNCs, it is hypothesized that such thermal stability improvements in A-PNCs could be attributed to the presence of an interphase over a great extent of the surface areas. Quasi-static nanoindentation testing revealed that the effective indentation and storage moduli of A-PNCs with transversely-oriented and longitudinally-oriented CNTs (T-CNTs and L-CNTs, respectively) exceeded those of the PUU baselines for both PUU211 and PUU541. PUU A-PNCs exhibit enhanced longitudinal effective indentation moduli of ~460 MPa (>3 × that of the PUU211 baseline) and ~1350 MPa (~1.5 × that of the PUU541 baseline) for L-CNT/PUU211 and L-CNT/PUU541 A-PNCs respectively. Smaller enhancements are seen in T-CNT/PUU A-PNCs, which exhibit enhanced transverse effective indentation moduli of ~210 MPa (~1.4 × that of the PUU211 baseline) and ~1040 MPa (~1.1 × that of the PUU541 baseline) for T-CNT/PUU211 and T-CNT/PUU541 A-PNCs, respectively. Greater enhancement is seen in the softer PUU211 materials than the PUU541 materials due to the stiffness mismatch between PUU211 and the CNTs, permitting a greater loading contribution from the CNTs. Furthermore, the mechanical enhancement in the L-CNT/PUU PNCs is up to 3 × greater than predicted by rule of mixtures analysis of PUU reinforced by wavy CNTs, indicating synergistic improvements *via* ordering and re-organization of hard-segment nanophases. PUU materials exhibit a rate sensitivity which is more pronounced in the PUU211 materials due to the larger and more rate-sensitive soft segment content. The hard-segment nanophases that self-organized in an orientation parallel to the CNT alignment direction might also play a significant role in these enhancements. Consequently, greater rate sensitivity is seen in T-CNT/PUU A-PNCs than in L-CNT/PUU A-PNCs due to the matrix-dominated loading of T-CNT/PUU A-PNCs. Additionally, increasing the concentration of the hard phase in PUU541 could presumably lead to an interconnected network of hard segments, where the corresponding influence on mechanical enhancement is manifested *via* the interphase throughout the interconnected A-CNT/PUU A-PNC architecture. Since there are a number of recent studies that quantified and modeled the mechanical response of viscoelastic polymers [62–64], and recent work has illustrated that confinement by A-CNTs of similar morphology and packing density can lead to enhanced mechanical properties of their composites due to meso-scale evolution of carbon crystallites that compose the matrix [4,65,66], further experimental and theoretical work on how the A-CNTs alter the morphogenesis of PUU and their resulting process-structure-mechanical property relations is needed. Additionally, since the A-CNTs used here had an inter-CNT spacing ~60–80 nm [35,37], which is much larger than the characteristic diameters of the soft and hard segments, future work utilizing A-

CNTs at higher packing densities (>20 vol %) is necessary. This study illustrates how A-CNTs could be utilized to tune the physical properties of PUU, and once analytical and numerical modeling tools which quantify and predict the impact of A-CNT packing on the soft- and hard segment morphology and orientation are available, accelerated design and fabrication of lightweight, strong, tough, and hard PUU A-PNC films for high-value structural applications could be enabled.

## Acknowledgments

This project was supported in part by an appointment to the Research Participation Program at the U.S. Army Research Laboratory administered by the Oak Ridge Institute for Science and Education through an interagency agreement between the U.S. Department of Defense and the EPA. This work was also supported by Airbus, Embraer, Lockheed Martin, Saab AB, Hexcel, Saertex, TohoTenax, and ANSYS through MIT's Nano-Engineered Composite Aerospace STructures (NECST) Consortium, and was supported in part by the U.S. Army Research Laboratory and the U. S. Army Research Office through the Institute of Soldier Nanotechnologies, under contract number W911NF-13-D-0001.

## Appendix A. Supplementary data

Supplementary data related to this article can be found at https://doi.org/10.1016/j.compscitech.2018.02.011.

## References

[1] G. Toader, E. Rusen, M. Teodorescu, A. Diacon, P.O. Stanescu, T. Rotariu, A. Rotariu, Novel polyurea polymers with enhanced mechanical properties, J. Appl. Polym. Sci. 133 (38) (2016), 43967.
[2] N. Iqbal, M. Tripathi, S. Parthasarathy, D. Kumar, P.K. Roy, "Polyurea coatings for enhanced blast-mitigation: a review, RSC Adv. 6 (111) (2016) 109706–109717.
[3] G. Toader, E. Rusen, M. Teodorescu, A. Diacon, P.O. Stanescu, C. Damian, T. Rotariu, A. Rotariu, New polyurea MWCNTs nanocomposite films with enhanced mechanical properties, J. Appl. Polym. Sci. 134 (28) (2017), 45061 .
[4] I.Y. Stein, A.L. Kaiser, A.J. Constable, L. Acauan, B.L. Wardle, Meso-scale evolution of non-graphitizing pyrolytic carbon in aligned carbon nanotube carbon matrix nanocomposites, J. Mater. Sci. 52 (24) (2017) 13799–13811.
[5] J. Shim, D. Mohr, Using split Hopkinson pressure bars to perform large strain compression tests on polyurea at low, intermediate and high strain rates, Int. J. Impact Eng. 36 (9) (Sep. 2009) 1116–1127.
[6] S.N. Raman, T. Ngo, J. Lu, P. Mendis, Experimental investigation on the tensile behavior of polyurea at high strain rates, Mater. Des. 50 (2013) 124–129.
[7] J.L. Abot, T. Alosh, K. Belay, Strain dependence of electrical resistance in carbon nanotube yarns, Carbon N. Y. 70 (Apr. 2014) 95–102.
[8] J.L. Abot, Y. Song, M.S. Vatsavaya, S. Medikonda, Z. Kier, C. Jayasinghe, N. Rooy, V.N. Shanov, M.J. Schulz, Delamination detection with carbon nanotube thread in self-sensing composite materials, Compos. Sci. Technol. 70 (7) (2010) 1113–1119.
[9] K.E. Strawhecker, A.J. Hsieh, T.L. Chantawansri, Z.I. Kalcioglu, K.J. Van Vliet, "Influence of microstructure on micro-/nano-mechanical measurements of select model transparent poly(urethane urea) elastomers, Polymer (Guildf). 54 (2) (Jan. 2013) 901–908.
[10] M. Grujicic, W.C. Bell, B. Pandurangan, T. He, Blast-wave impact-mitigation capability of polyurea when used as helmet suspension-pad material, Mater. Des. 31 (9) (2010) 4050–4065.
[11] J. Volder, M. Tawfick, S. Baughman, R. Hart, Carbon nanotubes: present and future commercial applications, Science (80-. ). 339 (2013) 535–539.
[12] N. Domun, H. Hadavinia, T. Zhang, T. Sainsbury, G.H. Liaghat, S. Vahid, "Improving the fracture toughness and the strength of epoxy using nanomaterials – a review of the current status, Nanoscale 7 (23) (2015) 10294–10329.
[13] A.K. Naskar, J.K. Keum, R.G. Boeman, Polymer matrix nanocomposites for automotive structural components, Nat. Nanotechnol. 11 (12) (2016) 1026–1030.
[14] B.L. Wardle, D.S. Saito, E.J. García, A.J. Hart, R. Guzmán De Villoria, E.A. Verploegen, Fabrication and characterization of ultrahigh-volume-fraction aligned carbon nanotube-polymer composites, Adv. Mater. 20 (2008) 2707–2714.
[15] F.H. Gojny, M.H.G. Wichmann, U. Köpke, B. Fiedler, K. Schulte, Carbon nanotube-reinforced epoxy-composites: enhanced stiffness and fracture toughness at low nanotube content, Compos. Sci. Technol. 64 (no. 15) (2004) 2363–2371.
[16] J.M. Cervantes-Uc, J.I.M. Espinosa, J.V. Cauich-Rodríguez, A. Ávila-Ortega, H. Vázquez-Torres, A. Marcos-Fernández, J.S. Román, TGA/FTIR studies of segmented aliphatic polyurethanes and their nanocomposites prepared with commercial montmorillonites, Polym. Degrad. Stabil. 94 (10) (2009) 1666–1677.
[17] J. Lee, I.Y. Stein, S.S. Kessler, B.L. Wardle, Aligned carbon nanotube film enables thermally induced state transformations in layered polymeric materials, ACS Appl. Mater. Interfaces 7 (16) (2015) 8900–8905.
[18] Y.F. Zhou, S. Xie, C.H. Chen, Pyrolytic polyurea encapsulated natural graphite as anode material for lithium ion batteries, Electrochim. Acta 50 (24) (Aug. 2005) 4728–4735.
[19] J.N. Coleman, U. Khan, Y.K. Gun'ko, Mechanical reinforcement of polymers using carbon nanotubes, Adv. Mater. 18 (6) (2006) 689–706.
[20] J.N. Coleman, M. Cadek, K.P. Ryan, A. Fonseca, J.B. Nagy, W.J. Blau, M.S. Ferreira, Reinforcement of polymers with carbon nanotubes. The role of an ordered polymer interfacial region. Experiment and modeling, Polymer (Guildf). 47 (2006) 8556–8561.
[21] A.J. Clancy, D.B. Anthony, S.J. Fisher, H.S. Leese, C.S. Roberts, M.S.P. Shaffer, T.S. Miller, S.A. Hodge, N.T. Skipper, V. Tileli, C.A. Howard, S. Enouz, M. Pasquali, Y.T. Zhu, Reductive dissolution of supergrowth carbon nanotubes for tougher nanocomposites by reactive coagulation spinning, Nanoscale 9 (25) (2017) 8764–8773.
[22] G. Pagani, M.J. Green, P. Poulin, M. Pasquali, Competing mechanisms and scaling laws for carbon nanotube scission by ultrasonication, Proc. Natl. Acad. Sci. 109 (29) (2012) 11599–11604.
[23] J. Stegen, Mechanics of carbon nanotube scission under sonication, J. Chem. Phys. 140 (no. 24) (2014), 244908.
[24] C.A. Amadei, I.Y. Stein, G.J. Silverberg, B.L. Wardle, C.D. Vecitis, Fabrication and morphology tuning of graphene oxide nanoscrolls, Nanoscale 8 (12) (2016) 6783–6791.
[25] L. Hu, D.S. Hecht, G. Gru, Carbon Nanotube Thin Films : Fabrication, Properties, and Applications, 2010, pp. 5790–5844.
[26] Y. He, X. Zhang, J. Runt, The role of diisocyanate structure on microphase separation of solution polymerized polyureas, Polym. (United Kingdom) 55 (3) (2014) 906–913.
[27] S.S. Sarva, S. Deschanel, M.C. Boyce, W. Chen, Stress–strain behavior of a polyurea and a polyurethane from low to high strain rates, Polymer (Guildf) 48 (8) (Apr. 2007) 2208–2213.
[28] R.G. Rinaldi, a. J. Hsieh, M.C. Boyce, Tunable microstructures and mechanical deformation in transparent poly(urethane urea)s, J. Polym. Sci., Part B: Polym. Phys. 49 (2) (Jan. 2011) 123–135.
[29] S.S. Sarva, A.J. Hsieh, The effect of microstructure on the rate-dependent stress–strain behavior of poly(urethane urea) elastomers, Polymer (Guildf). 50 (13) (Jun. 2009) 3007–3015.
[30] T.L. Chantawansri, Y.R. Sliozberg, J.W. Andzelm, A.J. Hsieh, Coarse-grained modeling of model poly(urethane urea)s: microstructure and interface aspects, Polymer (Guildf) 53 (20) (Sep. 2012) 4512–4524.
[31] A.M. Castagna, A. Pangon, T. Choi, G.P. Dillon, J. Runt, The role of soft segment molecular weight on microphase separation and dynamics of bulk polymerized polyureas, Macromolecules 45 (20) (2012) 8438–8444.
[32] I.Y. Stein, N. Lachman, M.E. Devoe, B.L. Wardle, Exohedral physisorption of ambient moisture scales non-monotonically with fiber proximity in aligned carbon nanotube arrays, ACS Nano 8 (5) (2014) 4591–4599.
[33] J.L. Gair, Nanotube-matrix Interplay and Tunability in Ultrahigh Volume-fraction Aligned Carbon Nanotube Poly(Urethane-urea) Nanocomposites, Ph.D. Thesis, University of Maryland, College Park, 2017.
[34] D.S. Jacobs, Constitutive Model of Aligned Carbon Nanotube/nafion Nanocomposite Ionic Electroactive Polymer Actuators, Master's Thesis, Archival, Massachusetts Institute of Technology, 2016, http://hdl.handle.net/1721.1/103529.
[35] J. Lee, I.Y. Stein, M.E. Devoe, D.J. Lewis, N. Lachman, S.S. Kessler, S.T. Buschhorn, B.L. Wardle, Impact of carbon nanotube length on electron transport in aligned carbon nanotube networks, Appl. Phys. Lett. 106 (5) (2015), 053110.
[36] I.Y. Stein, B.L. Wardle, Morphology and processing of aligned carbon nanotube carbon matrix nanocomposites, Carbon N. Y. 68 (2014) 807–813.
[37] I.Y. Stein, B.L. Wardle, Coordination number model to quantify packing morphology of aligned nanowire arrays, Phys. Chem. Chem. Phys. 15 (11) (2013) 4033–4040.
[38] I.Y. Stein, D.J. Lewis, B.L. Wardle, Aligned carbon nanotube array stiffness from stochastic three-dimensional morphology, Nanoscale 7 (46) (2015) 19426–19431.
[39] I.Y. Stein, B.L. Wardle, Packing morphology of wavy nanofiber arrays, Phys. Chem. Chem. Phys. 18 (2) (2016) 694–699.
[40] H.K. Mutha, Y. Lu, I.Y. Stein, H.J. Cho, M.E. Suss, Porosimetry and packing morphology of vertically aligned carbon nanotube arrays via impedance spectroscopy, Nanotechnology 28 (2017) 05LT01.
[41] Z. Petrovic, Z. Zavargo, J. Flynn, W. Macknight, Thermal degradation of MDI-based segmented polyurethanes, J. Appl. Polym. Sci. 51 (1994) 1087–1095.
[42] B. Fernández-d'Arlas, U. Khan, L. Rueda, J.N. Coleman, I. Mondragon, M. a. Corcuera, A. Eceiza, Influence of hard segment content and nature on polyurethane/multiwalled carbon nanotube composites, Compos. Sci. Technol. 71 (2011) 1030–1038.

[43] R. Sattar, A. Kausar, M. Siddiq, Advances in thermoplastic polyurethane composites reinforced with carbon nanotubes and carbon nanofibers: a review, J. Plast. Film Sheeting 31 (2) (2014) 186–224.
[44] Y. Wang, R. Song, Y. Li, J. Shen, Understanding tapping-mode atomic force microscopy data on the surface of soft block copolymers, Surf. Sci. 530 (3) (2003) 136–148.
[45] H. Sakamoto, H. Asakawa, T. Fukuma, S. Fujita, S.-I. Suye, Atomic force microscopy visualization of hard segment alignment in stretched polyurethane nanofibers prepared by electrospinning, Sci. Technol. Adv. Mater. 15 (15008) (2014), 015008.
[46] W. Hu, A.J. Hsieh, Phase-mixing and molecular dynamics in poly(urethane urea) elastomers by solid-state NMR, Polymer (Guildf) 54 (22) (Oct. 2013) 6218–6225.
[47] C. Oliver, M. Pharr, An improved technique for determining hardness and elastic modulus using load and displacement sensing indentation experiments, J. Mater. Res. 7 (11) (1992) 1564–1583.
[48] G. Feng, A.H.W. Ngan, Effects of creep and thermal drift on modulus measurement using depth-sensing indentation, J. Mater. Res. 17 (3) (2002) 660–668.
[49] D.P. Cole, J.C. Riddick, H.M. Iftekhar Jaim, K.E. Strawhecker, N.E. Zander, Interfacial mechanical behavior of 3D printed ABS, J. Appl. Polym. Sci. 133 (30) (2016), 43671.
[50] H. Cebeci, I.Y. Stein, B.L. Wardle, Effect of nanofiber proximity on the mechanical behavior of high volume fraction aligned carbon nanotube arrays, Appl. Phys. Lett. 104 (2) (2014), 023117.
[51] I.Y. Stein, B.L. Wardle, Mechanics of aligned carbon nanotube polymer matrix nanocomposites simulated via stochastic three-dimensional morphology, Nanotechnology 27 (3) (2016) 35701.
[52] P.M. Ajayan, L.S. Schadler, P.V. Braun, Nanocomposite Science and Technology, Wiley-VCH, 2003.
[53] C.M. McCarter, R.F. Richards, S.D. Mesarovic, C.D. Richards, D.F. Bahr, D. McClain, J. Jiao, Mechanical compliance of photolithographically defined vertically aligned carbon nanotube turf, J. Mater. Sci. 41 (23) (2006) 7872–7878.
[54] A.A. Zbib, S.D. Mesarovic, E.T. Lilleodden, D. McClain, J. Jiao, D.F. Bahr, The coordinated buckling of carbon nanotube turfs under uniform compression, Nanotechnology 19 (17) (2008) 175704.
[55] A. Qiu, D.F. Bahr, A.A. Zbib, A. Bellou, S.D. Mesarovic, D. McClain, W. Hudson, J. Jiao, D. Kiener, M.J. Cordill, Local and non-local behavior and coordinated buckling of CNT turfs, Carbon N. Y. 49 (4) (2011) 1430–1438.
[56] C. Cao, A. Reiner, C. Chung, S.H. Chang, I. Kao, R.V. Kukta, C.S. Korach, Buckling initiation and displacement dependence in compression of vertically aligned carbon nanotube arrays, Carbon N. Y. 49 (10) (2011) 3190–3199.
[57] M. Bedewy, A.J. Hart, Mechanical coupling limits the density and quality of self-organized carbon nanotube growth, Nanoscale 5 (7) (2013) 2928–2937.
[58] M. Bedewy, Data-driven understanding of collective carbon nanotube growth by in situ characterization and nanoscale metrology, J. Mater. Res. 32 (1) (2017) 153–165.
[59] A.L. Kaiser, I.Y. Stein, K. Cui, B.L. Wardle, Process-morphology scaling relations quantify self-organization in capillary densified nanofiber arrays, Phys. Chem. Chem. Phys. 20 (2018) 3876–3881.
[60] B. Natarajan, N. Lachman, T. Lam, D. Jacobs, C. Long, M. Zhao, B.L. Wardle, R. Sharma, J.A. Liddle, The evolution of carbon nanotube network structure in unidirectional nanocomposites resolved by quantitative electron tomography, ACS Nano 9 (6) (2015) 6050–6058.
[61] D. Handlin, I.Y. Stein, R. Guzman De Villoria, H. Cebeci, E.M. Parsons, S. Socrate, S. Scotti, B.L. Wardle, Three-dimensional elastic constitutive relations of aligned carbon nanotube architectures, J. Appl. Phys. 114 (no. 22) (2013).
[62] Q. Zhao, H.J. Qi, T. Xie, Recent progress in shape memory polymer: new behavior, enabling materials, and mechanistic understanding, Prog. Polym. Sci. 49–50 (2015) 79–120.
[63] J. Diani, P. Gilormini, C. Frédy, I. Rousseau, Predicting thermal shape memory of crosslinked polymer networks from linear viscoelasticity, Int. J. Solid Struct. 49 (5) (2012) 793–799.
[64] C. Gamonpilas, R. McCuiston, A non-linear viscoelastic material constitutive model for polyurea, Polymer (Guildf) 53 (17) (Aug. 2012) 3655–3658.
[65] J. Hu, Y. Zhu, H. Huang, J. Lu, Recent advances in shape–memory polymers: structure, mechanism, functionality, modeling and applications, Prog. Polym. Sci. 37 (12) (Dec. 2012) 1720–1763.
[66] I.Y. Stein, A.J. Constable, N. Morales-Medina, C.V. Sackier, M.E. Devoe, H.M. Vincent, B.L. Wardle, Structure-mechanical property relations of non-graphitizing pyrolytic carbon synthesized at low temperatures, Carbon N. Y. 117 (2017) 411–420.

# Supplementary Materials:

# Strong Process-Structure Interaction in Stoveable Poly(Urethane-Urea) Aligned Carbon Nanotube Nanocomposites

Jeffrey L. Gair Jr.[a,b,c], Robert H. Lambeth[d], Daniel P. Cole[a], Dale L. Lidston[c], Itai Y. Stein[c], Estelle Kalfon-Cohen[c], Alex J. Hsieh[d], Hugh A. Bruck[b], Mark L. Bundy[a], Brian L. Wardle[c]

[a]U.S. Army Research Laboratory, RDRL-VTM, Aberdeen Proving Ground, MD 21005-5069, USA
[b]Department of Mechanical Engineering, University of Maryland, College Park, MD 20742, USA
[c]Department of Aeronautics and Astronautics, Massachusetts Institute of Technology, Cambridge, MA 02139, USA
[d]U.S. Army Research Laboratory, RDRL-WMM, Aberdeen Proving Ground, MD 21005-5069, USA

# S1: AFM Height and Phase Maps for PUU541

The following figures are AFM height and phase images of PUU541 materials, namely the neat matrix ((a) and (b)), the T-CNT A-PNC ((c) and (d)), and the L-CNT A-PNC ((e) and (f)). These images supplement  Figure and the discussion of A-CNT effects on phase separation and sizes of *in situ* polymerized PUU, which is discussed in the main body of the manuscript in Section **Error! Reference source not found.**.

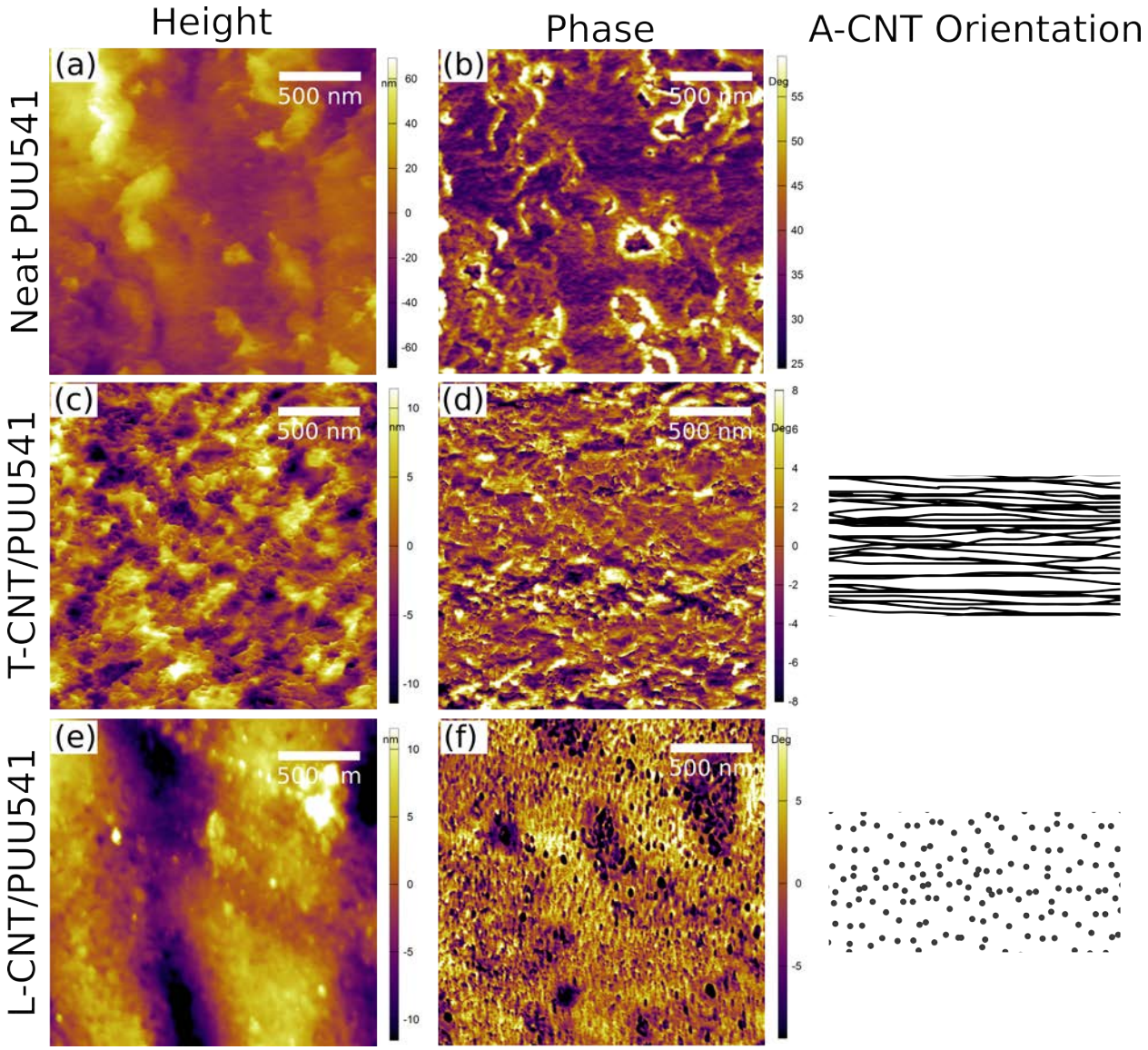


Figure S1: Representative AFM height (in nm) and phase (in degrees) images: PUU541 (a) height, (b) phase; T-CNT/PUU541 (c) height, (d) phase; L-CNT/PUU541 (e) height, (f) phase.

## S2: Tabulated Quasi-Static Nanoindentation Data

Table S1 contains summary data for all quasi-static nanoindentation tests completed. This tabulated format is intended to supplement  Figure and the subsequent discussion in Section **Error! Reference source not found.** of the manuscript.

Table S1: Summary of quasi-static nanoindentation data for all materials tested.

## S3: Dynamic Nanoindentation Loss Data

Figure S2 contains dynamic nanoindentation plots for the loss moduli of PUU211 materials (a) and PUU541 materials (b) from 1 to 200 Hz. The inclusion of the dynamic loss data is intended to aid discussion in Section **Error! Reference source not found.** and enhance Figure.

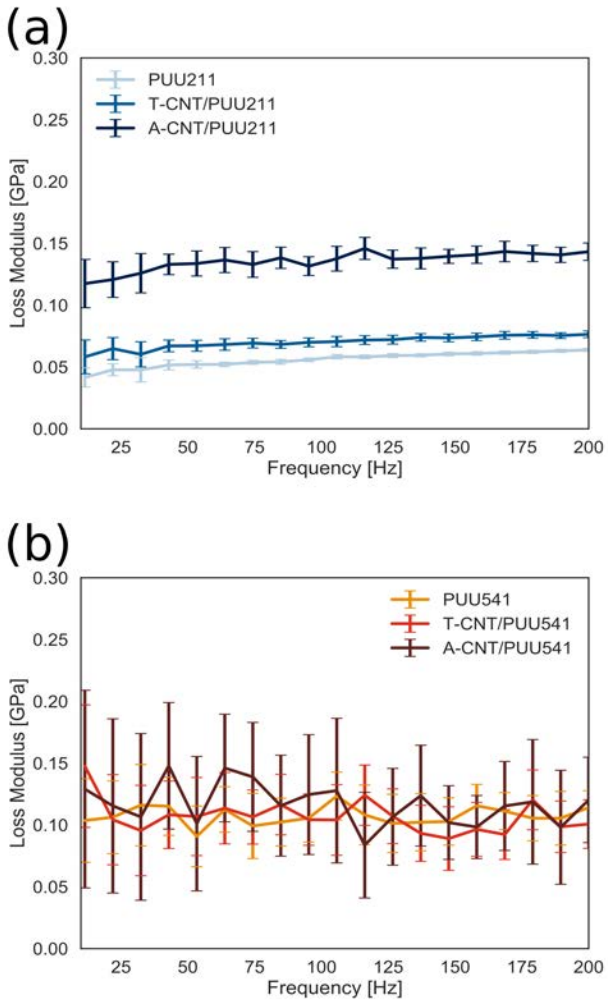


Figure S2: Summary of dynamic nanoindentation loss modulus data with standard error for (a) PUU211 and (b) PUU541 baseline and PNC materials. (Error bars are based on standard error from 54 test positions).